PARAMETER ESTIMATION FOR THE REDUCED FRACTURE MODEL VIA A DIRECT FILTER METHOD

Phuoc Toan Huynh,[1,*] Feng Bao,[1] & Thi-Thao-Phuong Hoang[2]

[1]*Department of Mathematics, Florida State University, Florida 32304, USA*

[2]*Department of Mathematics and Statistics, Auburn University, 221 Roosevelt Concourse, Auburn, Alabama 36849, USA*

*Address all correspondence to: Phuoc Toan Huynh, Department of Mathematics, Florida State University, Florida 32304, USA; Tel.: +1 470 529 6225, E-mail: th24ba@fsu.edu

In this work, we present a numerical method that provides accurate real-time detection for the widths of the fractures in a fractured porous medium based on observational data on porous medium fluid mass and velocity. To achieve this task, an inverse problem is formulated by first constructing a forward formulation based on the reduced fracture model of the diffusion equation. A parameter estimation problem is then performed online by utilizing a direct filter method. Numerical experiments are carried out to demonstrate the accuracy of our method in approximating the target parameters.

KEY WORDS: *reduced fracture model, mixed finite elements, inverse problem, parameter estimation, data assimilation, particle filtering*

1. INTRODUCTION

Fluid flow and transport problems in fractured porous media have many important applications in various fields such as subsurface hydrology, geophysics, and reservoir geomechanics. Therefore, it is necessary to have accurate and robust numerical simulations for such problems. However, such a task is often challenging due to the presence of the fractures. In particular, a fracture can represent either a fast pathway or a geological barrier, depending on whether its permeability is much higher or much lower than the surrounding rock matrix. In addition, the width of the fracture is much smaller than the size of the domain of calculation and any reasonable spatial mesh size. This issue requires refining the mesh locally around the fracture after imposing a global mesh on the entire domain, which is known to be computationally inefficient. One effective way to deal with this situation is to treat the fractures as interfaces, which avoids local refinement around the fractures. The original problem is then transformed into a new one where the interaction between the fractures and the surrounding rock matrix is taken into account [see Alboin et al. (1999, 2002), Amir et al. (2021), Angot et al. (2009), Fumagalli and Scotti (2011), Gander et al. (2021), Jaffre et al. (2005), Kadeethum et al. (2020), Morales and Showalter (2012) and the references therein]. Models with such low-dimensional fractures are known as reduced fracture models or mixed-dimensional models. Moreover, these models facilitate the use of different time scales in the fracture and in the rock matrix via a multi-scale approach, such as global-in-time domain decomposition methods (Hoang et al., 2013, 2016, 2017; Huynh et al., 2023a,b, 2024).

It is well known that the characteristics of the fractures significantly influence fluid flow patterns and the selection of numerical algorithms. Thus, in this work, we consider the following inverse problem: given the observations on the flow of the fluid in the fractured porous media,

Submitted: 9/21/24; Accepted: 10/28/24; Online: 11/12/24
https://doi.org/10.1615/JMachLearnModelComput.2024056400
2689–3967/25/$35.00

how can we infer the properties of the fractures, such as their widths? This is a practically important problem for engineers who seek to gain knowledge of the fractures when the observable data on the underground water is often limited. Such information will be invaluable when developing reliable models of naturally fractured reservoirs in order to optimize the primary and enhanced oil recovery methods. The study of inversion schemes for state and parameter estimation in flow and transport in (fractured) porous media is challenging and has attracted great attention of researchers (Ameur et al., 2002; Dai and Samper, 2004; Goc et al., 2010; Gwo, 2001; Krause et al., 2013; Mauldon et al., 1993; Neuman and Yakowitz, 1979; Renshaw, 1996; Wei and Rabinovich, 2023). However, limited work exists for the inverse problems associated with reduced fracture models. In Ameur et al. (2018), an iterative algorithm was proposed for the steady-state problem to estimate the location and hydrogeological properties of a small number of lower-dimensional fractures in a porous medium using given distributed pressure or flow data.

In this work, the fracture widths are considered as the parameter of interest, and the parameters detection problem we shall construct is based on a reduced fracture model of compressible fluid flow in which the fracture has larger permeability than the surrounding porous medium. One benefit of using the reduced fracture model is that one can include the fracture widths in the state estimation system, which facilitates the parameter estimation process. We aim to infer the widths of the fractures based on the real-time measurements of the porous media flow. To this end, the forward reduced fracture system is first implemented by using first-order backward Euler and mixed finite element methods (Boffi et al., 2013; Brezzi and Fortin, 1991; Roberts and Thomas, 1991), which are mass conservative and can handle heterogeneous and anisotropic diffusion tensors effectively. Next, to solve the inverse problem, we develop an online estimation method for the parameters representing the fractures widths. To achieve this goal, we utilize a direct filter method (Archibald et al., 2019; Cogan et al., 2021; Sun et al., 2023) to dynamically estimate the unknown parameters as we receive the observational data in an online manner. The main idea of the direct filter method is to incorporate the physical model with the observations on the state process through the likelihood and use Bayesian inference to project the observational data onto the parameter space. Preliminary research has shown that the direct filter method can accurately estimate the parameters for high dimensional data assimilation (Archibald and Bao, 2022; Archibald et al., 2019) and can be applied to solve practical problems (Cogan et al., 2021; Dyck et al., 2021; Sun et al., 2023). We remark that the model problem presented in this work is not complex, and our primary goal is to demonstrate the performance of the direct filter method for flows in fractured porous media. Thus, a multi-scale approach for the time discretization is not required here.

The rest of this paper is organized as follows: in Section 2, we introduce the model problem, formulate the corresponding reduced fracture model, and derive its fully discrete version. We shall discuss the optimal filtering for online parameter estimation in Section 3. The direct filter method and its implementation are also introduced. In Section 4, we discuss how to apply the direct filter method to estimate the target parameter in the reduced fracture model. Numerical experiments will also be carried out to illustrate the performance of the direct filter approach. The paper is then closed with a conclusion section.

2. REDUCED FRACTURE MODEL FOR THE DIFFUSION EQUATIONS

Let Ω be a bounded domain in $\mathbb{R}^2$ with Lipschitz boundary $\partial\Omega$ and $T > 0$ be some fixed time. Consider the flow problem of a single-phase, compressible fluid written in mixed form as follows:

$$\begin{aligned} \phi\partial_t p + \operatorname{div} \boldsymbol{u} &= q && \text{in } \Omega \times (0,T), \\ \boldsymbol{u} &= -\boldsymbol{K}\nabla p && \text{in } \Omega \times (0,T), \\ p &= 0 && \text{on } \partial\Omega \times (0,T), \\ p(\cdot,0) &= p_0 && \text{in } \Omega, \end{aligned} \tag{1}$$

where p is the pressure, $\boldsymbol{u}$ is the velocity, q is the source term, ϕ is the storage coefficient, and $\boldsymbol{K}$ is a symmetric, time-independent, hydraulic conductivity tensor. Suppose that the fracture Ω_f is a subdomain of Ω, whose thickness is d, that separates Ω into two connected subdomains: $\Omega \backslash \overline{\Omega}_f = \Omega_1 \cup \Omega_2$, and $\Omega_1 \cap \Omega_2 = \emptyset$. For simplicity, we assume further that Ω_f can be expressed as

$$\Omega_f = \left\{ \boldsymbol{x} \in \Omega : \boldsymbol{x} = \boldsymbol{x}_\gamma + s\boldsymbol{n} \text{ where } \boldsymbol{x}_\gamma \in \gamma \text{ and } s \in \left(-\frac{d}{2}, \frac{d}{2}\right) \right\},$$

where γ is the intersection between a line with Ω (see Fig. 1).

We denote by γ_i the part of the boundary of Ω_i shared with the boundary of the fracture Ω_f: $\gamma_i = (\partial\Omega_i \cap \partial\Omega_f) \cap \Omega$, for $i = 1, 2$. Let $\boldsymbol{n}_i$ be the unit, outward pointing, normal vector field on $\partial\Omega_i$, where $\boldsymbol{n} = \boldsymbol{n}_1 = -\boldsymbol{n}_2$. For $i = 1,\ 2,\ f$, and for any scalar, vector, or tensor-valued function φ defined on Ω, we denote by φ_i the restriction of φ to Ω_i. The original problem (1) can be rewritten as the following transmission problem:

$$\begin{aligned} \phi_i\partial_t p_i + \operatorname{div} \boldsymbol{u}_i &= q_i && \text{in } \Omega_i \times (0,T), && i = 1,2,f, \\ \boldsymbol{u}_i &= -\boldsymbol{K}_i\nabla p_i && \text{in } \Omega_i \times (0,T), && i = 1,2,f, \\ p_i &= 0 && \text{on } (\partial\Omega_i \cap \partial\Omega) \times (0,T), && i = 1,2,f, \\ p_i &= p_f && \text{on } \gamma_i \times (0,T), && i = 1,2, \\ \boldsymbol{u}_i \cdot \boldsymbol{n}_i &= \boldsymbol{u}_f \cdot \boldsymbol{n}_i && \text{on } \gamma_i \times (0,T), && i = 1,2, \\ p_i(\cdot,0) &= p_{0,i} && \text{in } \Omega_i, && i = 1,2,f. \end{aligned} \tag{2}$$

The reduced fracture model that we consider in this paper was first proposed in Alboin et al. (1999, 2002) under the assumption that the fracture has larger permeability than that in the rock matrix. The model is obtained by averaging across the transversal cross sections of the two-dimensional fracture Ω_f. We use the notation ∇_τ and div_τ for the tangential gradient and tangential divergence, respectively. We write ϕ_γ and $\boldsymbol{K}_\gamma$ for $d\phi_f$ and $\boldsymbol{K}_{f,\tau}$, respectively, where $\boldsymbol{K}_{f,\tau}$ is the tangential component of $\boldsymbol{K}_f$. The reduced model consists of equations in the subdomains,

$$\begin{aligned} \phi_i\partial_t p_i + \operatorname{div} \boldsymbol{u}_i &= q_i && \text{in } \Omega_i \times (0,T), \\ \boldsymbol{u}_i &= -\boldsymbol{K}_i\nabla p_i && \text{in } \Omega_i \times (0,T), \\ p_i &= 0 && \text{on } (\partial\Omega_i \cap \partial\Omega) \times (0,T), \\ p_i &= p_\gamma && \text{on } \gamma \times (0,T), \\ p_i(\cdot,0) &= p_{0,i} && \text{in } \Omega_i, \end{aligned} \tag{3}$$

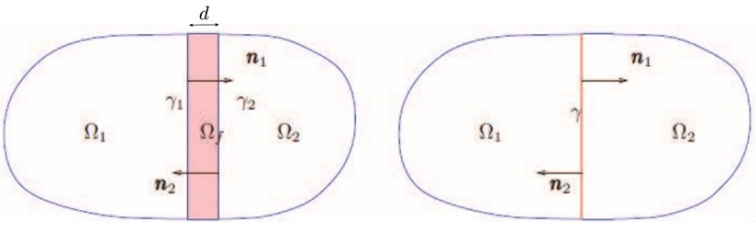

FIG. 1: The domain Ω with the fracture Ω_f (left) and the fracture-interface γ (right)

for $i = 1, 2$, and equations in the fracture-interface γ,

$$\begin{aligned} \phi_\gamma \partial_t p_\gamma + \mathrm{div}_\tau \boldsymbol{u}_\gamma &= q_\gamma + \sum_{i=1}^{2} (\boldsymbol{u}_i \cdot \boldsymbol{n}_i)_{|\gamma} && \text{in } \gamma \times (0,T), \\ \boldsymbol{u}_\gamma &= -\boldsymbol{K}_\gamma d \nabla_\tau p_\gamma && \text{in } \gamma \times (0,T), \\ p_\gamma &= 0 && \text{on } \partial\gamma \times (0,T), \\ p_\gamma(\cdot, 0) &= p_{0,\gamma} && \text{in } \gamma, \end{aligned} \tag{4}$$

where p_γ, $\boldsymbol{u}_\gamma$, and q_γ are the reduced pressure, flux, and the source term, respectively, which are given by

$$p_\gamma = \frac{1}{d} \int_{-d/2}^{d/2} p_f(x_\gamma + s\boldsymbol{n}) ds, \quad \boldsymbol{u}_\gamma = \int_{-d/2}^{d/2} \boldsymbol{u}_{f,\tau}(x_\gamma + s\boldsymbol{n}) ds, \quad q_\gamma = \int_{-d/2}^{d/2} q_f(x_\gamma + s\boldsymbol{n}) ds,$$

where $\boldsymbol{u}_{f,\tau}$ is the tangential component of $\boldsymbol{u}_f$. To write the weak formulation of Eqs. (3) and (4), we use the convention that if V is a space of functions, then $\boldsymbol{V}$ is a space of vector functions having each component in V. For arbitrary domain $\mathcal{O}$, we denote by $(\cdot,\cdot)_{\mathcal{O}}$ the inner product in $L^2(\mathcal{O})$ or $\boldsymbol{L}^2(\mathcal{O})$. We next define the following Hilbert spaces:

$$\begin{aligned} M &= \big\{ v = (v_1, v_2, v_\gamma) \in L^2(\Omega_1) \times L^2(\Omega_2) \times L^2(\gamma) \big\}, \\ \Sigma &= \Big\{ \boldsymbol{v} = (\boldsymbol{v}_1, \boldsymbol{v}_2, \boldsymbol{v}_\gamma) \in \boldsymbol{L}^2(\Omega_1) \times \boldsymbol{L}^2(\Omega_2) \times \boldsymbol{L}^2(\gamma) : \ \mathrm{div}\, \boldsymbol{v}_i \in L^2(\Omega_i), \ \ i = 1, 2, \\ &\qquad \text{and} \quad \mathrm{div}_\tau\, \boldsymbol{v}_\gamma - \sum_{i=1}^{2} \boldsymbol{v}_i \cdot \boldsymbol{n}_{i|\gamma} \in L^2(\gamma) \Big\}. \end{aligned}$$

We define the bilinear forms $a(\cdot,\cdot;d)$, $b(\cdot,\cdot)$, and $c(\cdot,\cdot)$ on $\Sigma \times \Sigma$, $\Sigma \times M$, and $M \times M$, respectively, and the linear form L_q on M by

$$\begin{aligned} a(\boldsymbol{u}, \boldsymbol{v}; d) &= \sum_{i=1}^{2} \big(\boldsymbol{K}_i^{-1} \boldsymbol{u}_i, \boldsymbol{v}_i \big)_{\Omega_i} + \Big((\boldsymbol{K}_\gamma d)^{-1} \boldsymbol{u}_\gamma, \boldsymbol{v}_\gamma \Big)_\gamma, \\ b(\boldsymbol{u}, \mu) &= \sum_{i=1}^{2} (\mathrm{div}\, \boldsymbol{u}_i, \mu_i)_{\Omega_i} + \left(\mathrm{div}_\tau\, \boldsymbol{u}_\gamma - \sum_{i=1}^{2} \boldsymbol{u}_i \cdot \boldsymbol{n}_{i|\gamma}, \mu_\gamma \right)_\gamma, \\ c_\phi(\eta, \mu) &= \sum_{i=1}^{2} (\phi_i \eta_i, \mu_i)_{\Omega_i} + (\phi_\gamma \eta_\gamma, \mu_\gamma)_\gamma, \quad L_q(\mu) = \sum_{i=1}^{2} (q_i, \mu_i)_{\Omega_i} + (q_\gamma, \mu_\gamma)_\gamma. \end{aligned} \tag{5}$$

The weak form of Eqs. (3) and (4) can be written as follows:

Find $p \in H^1(0,T;M)$ and $\boldsymbol{u} \in L^2(0,T;\Sigma)$ such that

$$\begin{aligned} a(\boldsymbol{u}, \boldsymbol{v}; d) - b(\boldsymbol{v}, p) &= 0 \forall \boldsymbol{v} \in \Sigma, \\ c_\phi(\partial_t p, \mu) + b(\boldsymbol{u}, \mu) &= L_q(\mu) \forall \mu \in M, \end{aligned} \tag{6}$$

together with the initial conditions:

$$p_i(\cdot, 0) = p_{0,i}, \ \text{in } \Omega_i, \ i = 1, 2, \quad \text{and} \quad p_\gamma(\cdot, 0) = p_{0,\gamma}, \ \text{in } \gamma. \tag{7}$$

The well-posedness of problem (6) and (7) was proved in Hoang et al. (2016). To find the numerical solutions to Eqs. (6) and (7), we discretize the problem in space using mixed finite

element method (Boffi et al., 2013; Brezzi and Fortin, 1991; Roberts and Thomas, 1991) and in time using backward Euler method. To this end, let $\mathcal{K}_{h,i}$ be a finite element partition of Ω_i $(i = 1, 2)$ into triangles. We denote by $\mathcal{G}_{h,i}$ the set of the edges of elements $\mathcal{K}_{h,i}$ lying on the interface γ. Since $\mathcal{K}_1$ and $\mathcal{K}_2$ coincide on γ, the spaces $\mathcal{G}_{h,1}$ and $\mathcal{G}_{h,2}$ are identical; thus we set $\mathcal{G}_h := \mathcal{G}_{h,1} = \mathcal{G}_{h,2}$. For $i = 1, 2$, we consider the lowest-order Raviart–Thomas mixed finite element spaces $M_{h,i} \times \Sigma_{h,i} \subset L^2(\Omega_i) \times H(\mathrm{div}, \Omega_i)$:

$$
\begin{aligned}
&M_{h,i} = \big\{\mu_{h,i} \in L^2(\Omega_i) :\ \mu_{h,i|K_i} = \text{const},\ \ \forall K_i \in \mathcal{K}_{h,i}\big\},\\
&\Sigma_{h,i} = \big\{\boldsymbol{v}_{h,i} \in H(\mathrm{div}, \Omega_i) :\ \boldsymbol{v}_{h,i|K_i} = (b_{K,i} + a_{K,i}x,\ c_{K,i} + a_{K,i}y),\\
&(a_{K,i},\ b_{K,i},\ c_{K,i}) \in \mathbb{R}^3, \quad \forall K_i \in \mathcal{K}_{h,i}\big\}.
\end{aligned}
$$

Similarly for the fracture, let $\Lambda_h \times \Sigma_{h,\gamma} \subset L^2(\gamma) \times H(\mathrm{div}_\tau, \gamma)$ be the lowest-order Raviart–Thomas spaces in one dimension:

$$
\begin{aligned}
&M_{h,\gamma} = \big\{\mu_{h,\gamma} \in L^2(\gamma) :\ \lambda_{|E} = \text{const},\ \forall E \in \mathcal{G}_h\big\},\\
&\Sigma_{h,\gamma} = \big\{\boldsymbol{v}_{h,\gamma} \in H(\mathrm{div}_\tau, \gamma) :\ \boldsymbol{v}_{h,\gamma|E} = az + b,\ (a,\ b) \in \mathbb{R}^2,\ \forall E \in \mathcal{G}_h\big\}.
\end{aligned}
$$

For the discretization in time, we consider a uniform partition of $(0,\ T)$ into N subintervals $(t^n,\ t^{n+1})$ of length $\Delta t = t^{n+1} - t^n$, for $n = 0, \ldots, N-1$. The time derivatives are approximated by the backward difference quotient

$$
\bar{\partial} c^n = \frac{c^n - c^{n-1}}{\Delta t}, \quad n = 1, \ldots, N,
$$

where the superscript n indicates the evaluation of a function at the discrete time $t = t^n$.

Finally, denote

$$
\boldsymbol{M}_h = M_{h,1} \times M_{h,2} \times M_{h,\gamma}, \qquad \boldsymbol{\Sigma}_h = \Sigma_{h,1} \times \Sigma_{h,2} \times \Sigma_{h,\gamma},
$$

the fully discrete version of Eqs. (6) and (7) reads as follows:

For $n = 1, \ldots, N$, find $(p_h^n, \boldsymbol{u}_h^n) \in \boldsymbol{M}_h \times \boldsymbol{\Sigma}_h$ satisfying

$$
\begin{aligned}
a(\boldsymbol{u}_h^n, \boldsymbol{v}_h; d) - b(\boldsymbol{v}_h, p_h^n) &= 0 \forall \boldsymbol{v}_h \in \boldsymbol{\Sigma}_h,\\
c_\Phi\big(\bar{\partial} p_h^n, \mu_h\big) + b(\boldsymbol{u}_h^n, \mu_h) &= L_q^n(\mu_h) \forall \mu_h \in \boldsymbol{M}_h,
\end{aligned}
\tag{8}
$$

together with the initial conditions:

$$
p_{h,i|K_i}^0 := \frac{1}{|K_i|}\int_{K_i} p_{0,i},\ \forall K_i \in \mathcal{K}_{h,i},\ i = 1, 2, \ \text{ and } \ p_{h,\gamma|E}^0 = \frac{1}{|E|}\int_E p_{0,\gamma},\ \forall E \in \mathcal{G}_h. \tag{9}
$$

3. DATA ASSIMILATION

In this section, we are interested in the following problems: given the observations on the solution of Eqs. (8) and (9), what can we say about the characteristics of the existing fractures? In particular, we aim to estimate the widths of the fractures provided some partial information of the solution. To address this question, we need to incorporate some techniques from data assimilation.

3.1 General Framework

We first briefly present the general framework of data assimilation. Suppose we have the following state-space model of a dynamical system

$$S_{n+1} = g(S_n) + \varepsilon_n, \quad n = 0, 1, \ldots, \tag{10}$$

where $g : \mathbb{R}^l \to \mathbb{R}^l$ is a given mathematical model (linear of nonlinear), and the term $\varepsilon_n \in \mathbb{R}^l$ is the noise in the system which is usually assumed to be Gaussian. The process $\{S_n\}_n$ is referred to as the state process, which is often not directly observable, and the available data one received typically consist of partial observations of the state S_n, which are given by

$$O_{n+1} = G(S_{n+1}) + \zeta_{n+1}, \quad n = 0, 1, \ldots. \tag{11}$$

The process $\{O_n\}_n \subset \mathbb{R}^k$ $(k \leq l)$ is called the observation process, and $G : \mathbb{R}^l \to \mathbb{R}^k$ could be either a linear or nonlinear function, and ζ_{n+1} is a Gaussian noise. The goal of the data assimilation is to obtain the best estimate for the state S_n given the observation process $\{O_i\}_{i=1}^n$. Mathematically, we need to find the optimal filer for S_n, denoted by $\bar{S}_n$ with

$$\bar{S}_n := \mathbb{E}[S_n | O_{1:n}]. \tag{12}$$

In this work, we use the Bayesian inference framework to obtain such estimation, which consists of two steps. The first step is the prediction step where the Chapman–Kolmogrov formula is applied to compute

$$p(S_{n+1}|O_{1:n}) = \int p(S_{n+1}|S_n)p(S_n|O_{1:n})dS_n, \tag{13}$$

where we assume that $p(S_n|O_{1:n})$ is known, and $p(S_{n+1}|S_n)$ is the transition kernel which can be computed by using Eq. (10).

The next step is to use the Bayes' formula to update the new posterior:

$$p(S_{n+1}|O_{1:n+1}) = \frac{p(O_{n+1}|S_{n+1})p(S_{n+1}|O_{1:n})}{p(O_{n+1}|O_{1:n})}. \tag{14}$$

As the given dynamical system is nonlinear in general, the terms occurring in Eqs. (13) and (14) may not have analytic expressions. The general idea to handle this difficulty is to construct an ensemble of particles, which represents a convex combination of Dirac measure, and iteratively update their locations and weights. As the number of particles increases, the conditional distribution is expected to converge to the exact distribution [see, e.g., Doucet et al. (2001b)]. This approach consists of the following steps: at time step n, assume we have a collection of particles $\{s_n^{(m)}\}_{m=1}^M$.

1. Approximate $p(S_n|O_{1:n})$ by the empirical distribution $\tilde{p}(S_n|O_{1:n})$ given by

$$\tilde{p}(S_n|O_{1:n}) = \sum_{m=1}^{M} w_n^{(m)} \delta_{s_n^{(m)}}(S_n), \tag{15}$$

   where $w_n^{(m)}$ stands for the weight of the particle s_n^m, which is given, and δ_x is the Dirac delta function at x.

2. For the prediction step, we first use the state equation (10) to generate M empirical particles $\tilde{s}_{n+1}^{(m)}$ satisfying

$$\tilde{s}_{n+1}^{(m)} = g(s_n^{(m)}) + \varepsilon_n^{(m)}, \quad m = 1, \ldots, M.$$

Those particles are used to compute the empirical distribution $\tilde{\pi}(S_{n+1}|O_{1:n})$, which is an approximation for $p(S_{n+1}|O_{1:n})$, through the Chapma–Kolmogrov formula:

$$\tilde{\pi}(S_{n+1}|O_{1:n}) = \sum_{m=1}^{M} w_n^{(m)} \delta_{\tilde{s}_{n+1}^{(m)}}(S_{n+1}). \tag{16}$$

3. The empirical distribution of the update step is given by the following relation:

$$\tilde{\pi}(S_{n+1}|O_{1:n+1}) := \sum_{m=1}^{M} w_{n+1}^{(m)} \delta_{\tilde{s}_{n+1}^{(m)}}(S_{n+1}), \tag{17}$$

where

$$w_{n+1}^{(m)} = \frac{\tilde{w}_{n+1}^{(m)}}{\sum_{m=1}^{M} \tilde{w}_{n+1}^{(m)}}, \quad \tilde{w}_{n+1}^{(m)} = p\Big(O_{n+1}|\tilde{s}_{n+1}^{(m)}\Big) w_n^{(m)}.$$

4. To avoid degeneracy, which means that a lot of the weights of the particles will be ignored, one needs a re-sampling step for the updated measure. This involves generating M samples from the distribution (17) and assigning a weight of $1/M$ to each of the particles. The goal of this step is to eliminate particles with small weights.

Since estimating the parameter d is our main focus, and the state estimates are unnecessary, we adopt the direct particle filter method, developed in Archibald et al. (2019). Such method will help us avoid unwanted distraction in the state estimation process and directly provide the approximations of the target parameter. As a consequence, the dimension of the problem is the same as the dimension of the parameter of interest, which would address the "curse of dimensionality" when solving nonlinear filtering problems in online parameter estimation (Archibald et al., 2019). Therefore, this method could solve the parameter estimation problem efficiently, especially for our case when the dimension of the state model is very high and the parameter d is a low-dimensional vector.

3.2 Direct Filter for Parameter Estimation

Similar to Eqs. (10) and (11), let $X_n \in \mathbb{R}^l$ describe the state of some physical model, and $Y_n \in \mathbb{R}^k$ is a noisy observation of X_n with a noise perturbation ξ_n. We also denote by $\theta \in \mathbb{R}^p$ $(p \ll l)$ the vector of target parameters and assume that we have the following system for the parameter estimation problem:

$$X_{n+1} = h(X_n,\ \theta) + w_n, \tag{18}$$

$$Y_{n+1} = HX_{n+1} + \xi_{n+1}, \tag{19}$$

where $h : \mathbb{R}^l \times \mathbb{R}^p \to \mathbb{R}^l$ is a function (linear or nonlinear) representing the considered physics model, $H : \mathbb{R}^l \to \mathbb{R}^k$ is a linear matrix, and (w_n, ξ_n) is a pair of independent Gaussian noises.

The parameter estimation problem we are interested in is to estimate θ in Eq. (18) by using the observational data Y provided in Eq. (19).

In the direct filter method, instead of treating θ as a vector containing deterministic constant entries, we consider θ as a stochastic process to be estimated with respect to time. To this end, we replace θ in Eq. (18) with θ_n and rewrite Eqs. (18) and (19) in the following form:

$$\theta_{n+1} = \theta_n + \epsilon_n, \tag{20}$$

$$Y_{n+1} = H(h(X_n,\ \theta_{n+1}) + w_n) + \xi_{n+1}, \tag{21}$$

where ϵ_n is an artificial dynamic noise. We define $\zeta_{n+1} = Hw_n + \xi_{n+1}$, which is a multivariate Gaussian variable, and we can obtain the following dynamics:

$$\theta_{n+1} = \theta_n + \epsilon_n, \tag{22}$$

$$Y_{n+1} = Hh(X_n,\ \theta_{n+1}) + \zeta_{n+1}. \tag{23}$$

We aim to find the best estimate $\mathbb{E}[\theta_n|Y_{1:n}]$ for θ_n at any time instant n given the observation process $\{Y_i\}_{i=1}^n$. Instead of generating a long-term simulation trajectory for the process of X_n [e.g., Kantas et al. (2015)], we follow the idea in Archibald et al. (2019) and use the fact that the observation data Y_n provides direct observations on X_n and introduce the following approximation scheme:

$$H^{-1}Y_n \approx H^{-1}(Y_n - \xi_n) = X_n,$$

which leads to the approximation dynamical system

$$\theta_{n+1} = \theta_n + \epsilon_n, \tag{24}$$

$$\tilde{Y}_{n+1} = Hh(H^{-1}\tilde{Y}_n,\ \theta_{n+1}) + \zeta_{n+1}. \tag{25}$$

We conclude this section by introducing the implementation of the direct filter method. More detailed discussions can be found in Archibald et al. (2019). This method is initialized by first generating a collection of M particles $\left\{\theta_n^{(m)}\right\}_{m=1}^M$ that describes $p(\theta_n|Y_{1:n})$ at time instant n and consists of the following three steps:

1. **The prediction step.** Generates a prior estimate $\tilde{\theta}_{n+1} = \left\{\tilde{\theta}_{n+1}^{(m)}\right\}_{m=1}^M$ for the target parameter θ_{n+1}, using Eq. (24) by adding $\left\{\epsilon_n^{(m)}\right\}_{m=1}^M$ to $\left\{\theta_n^{(m)}\right\}_{m=1}^M$:

   $$\tilde{\theta}_{n+1}^{(m)} = \theta_n^{(m)} + \epsilon_n^{(m)}, \quad m = 1, 2, \ldots, M.$$

   The prediction step provides an empirical distribution $\tilde{\pi}(\theta_{n+1}|Y_{1:n})$ for the prior $p(\theta_{n+1}|Y_{1:n})$, which is computed by

   $$\tilde{\pi}(\theta_{n+1}|Y_{1:n}) = \frac{1}{M}\sum_{m=1}^{M} \delta_{\tilde{\theta}_{n+1}^{(m)}}(\theta_{n+1}). \tag{26}$$

2. **The update step.** The update step incorporates the observational data and derives a weighted posterior distribution based on the prior $\tilde{\pi}(\theta_{n+1}|Y_{1:n})$ given in Eq. (26):

$$\tilde{\pi}(\theta_{n+1}|Y_{1:n+1}) = \frac{1}{C}\sum_{m=1}^{M} p\Big(Y_{n+1}|\tilde{\theta}_{n+1}^{(m)}\Big)\delta_{\tilde{\theta}_{n+1}^{(m)}}(\theta_{n+1}) = \sum_{m=1}^{M} w_{n+1}^{(m)}\delta_{\tilde{\theta}_{n+1}^{(m)}}(\theta_{n+1}), \quad (27)$$

where $w_{n+1}^{(m)} = p\Big(Y_{n+1}|\tilde{\theta}_{n+1}^{(m)}\Big)/C$ is the weight for the particle $\tilde{\theta}_{n+1}^{(m)}$ with a normalization factor C, and the likelihood function in Eq. (26) is given by

$$p\Big(Y_{n+1}|\tilde{\theta}_{n+1}^{(m)}\Big) = \exp\bigg(-\frac{1}{2}||Hh\Big(H^{-1}Y_n, \tilde{\theta}_{n+1}^{(m)}\Big) - Y_{n+1}||_R^2\bigg), \quad (28)$$

where $||\alpha||_R := \alpha R^{-1}\alpha$, with R standing for the invariance variance of the observational noise ζ_{n+1}.

3. **Resampling step.** The purpose of the resampling step is to generate a set of equally weighted samples to avoid the degeneracy issue (Archibald et al., 2019; Bao et al., 2014, 2018, 2019, 2020; Bao and Maroulas, 2017). In this work, we simply use the importance sampling method (Doucet et al., 2001a; Morzfeld et al., 2018) to generate samples, denoted by $\Big\{\theta_{n+1}^{(m)}\Big\}_{m=1}^{M}$, from the weighted importance distribution $\tilde{\pi}(\theta_{n+1}|Y_{1:n+1})$. More specifically, we use the distribution $\tilde{\pi}(\theta_{n+1}|Y_{1:n+1})$ to sample with replacement M particles $\Big\{\tilde{\theta}_{n+1}^{(m)}\Big\}_{m=1}^{M}$ according to the weights $\Big\{w_{n+1}^{(m)}\Big\}_{m=1}^{M}$ to obtain $\Big\{\theta_{n+1}^{(m)}\Big\}_{m=1}^{M}$. This way, we can replace particles with small weights by particles with large weights. We then obtain an "unweighted" empirical distribution as follows:

$$\tilde{p}(\theta_{n+1}|Y_{1:n+1}) = \frac{1}{M}\sum_{m=1}^{M}\delta_{\theta_{n+1}^{(m)}}(\theta_{n+1}),$$

and use $\tilde{p}(\theta_{n+1}|Y_{1:n+1})$ as the initial empirical distribution for the next time instant $n+1$.

With the above procedure, the estimate we obtain for the target parameter at the time instant $n+1$ is given by

$$\tilde{\theta} = \frac{1}{n+1-j}\sum_{i=j}^{n+1}\tilde{\mathbb{E}}[\theta_i|Y_{1:i}],$$

where j is a number of burn-in steps to reduce the influence of large noises at some time instants, and $\tilde{\mathbb{E}}[\theta_i|Y_{1:i}]$ is the mean estimate of the empirical distribution $\tilde{p}(\theta_i|Y_{1:i})$.

Remark 1. Throughout Section 4, the values of the perturbation noise $\{\epsilon_n\}$ in Eq. (20) will be chosen empirically. However, we note that there is a method for systematically selecting these values. Specifically, the authors in Liu and West (2001) used the kernel smoothing approach with location shrinkage developed in West (1993) to derive a relation between the variance matrix of the perturbed noise ϵ_{n+1} at time instant $n+1$ with the variance matrix of the particle parameters θ_n at the previous time step n. From this relation, we can determine the values of the noise.

4. NUMERICAL RESULTS

In this section, we shall explain how to apply the direct filter method to estimate the width of the fracture based on the fully discrete version of the reduced fracture model, i.e., the system of Eqs. (8) and (9). We then carry out some numerical experiments with different fracture configurations to demonstrate the performance of the method.

4.1 Problem Setup

To incorporate the direct filter algorithm, we first rewrite the system (8) and (9) in a more compact form. Let $\bar{\boldsymbol{M}}_h$ and $\bar{\boldsymbol{\Sigma}}_h$ be the finite collections of basis functions in $\boldsymbol{M}_h$ and $\boldsymbol{\Sigma}_h$, respectively. We introduce the following matrices resulted in the bi-linear forms given in Eq. (5):

$$\begin{aligned} \boldsymbol{A}_h(d) &= (a(\boldsymbol{r}_h, \boldsymbol{v}_h; d))_{\boldsymbol{r}_h, \boldsymbol{v}_h \in \bar{\boldsymbol{\Sigma}}_h}, \quad \boldsymbol{B}_h = (-b(\boldsymbol{v}_h, \eta_h))_{\boldsymbol{v}_h \in \bar{\boldsymbol{\Sigma}}_h, \eta_h \in \bar{\boldsymbol{M}}_h}, \\ \boldsymbol{C}_{h,\phi} &= (-c_\phi(\eta_h, \lambda_h))_{\eta_h, \lambda_h \in \bar{\boldsymbol{M}}_h}. \end{aligned} \tag{29}$$

By replacing v_h and μ_h in Eq. (8) by the basis functions and expressing $\boldsymbol{u}_h^n$ and p_h^n in terms of those basis functions, we obtain the following matrix form for Eq. (8):

$$\boldsymbol{\Lambda}_h(d) X_n = F(X_{n-1},\, \boldsymbol{G}_h), \tag{30}$$

where

$$\boldsymbol{\Lambda}_h(d) = \begin{bmatrix} \boldsymbol{A}_h(d) & \boldsymbol{B}_h \\ \Delta t (\boldsymbol{B}_h)^T & \boldsymbol{C}_{h,\phi}, \end{bmatrix}, \tag{31}$$

with Δt being the chosen timestep size, $\boldsymbol{G}_h$ is a vector containing the boundary conditions, and $X_n = (\boldsymbol{u}_h^n, p_h^n)$. Equivalently, we have the following recursive relation:

$$X_n = \boldsymbol{\Phi}(X_{n-1},\ d),\ n = 1, 2, \ldots, \tag{32}$$

where

$$\boldsymbol{\Phi}(X_{n-1}, d) = (\boldsymbol{\Lambda}(d))^{-1} F(X_{n-1},\, \boldsymbol{G}_h).$$

We can see that by using the reduced fracture model, the parameter of interest d is included in the state equation (32). Thus, the direct filter method can be applied to approximate d. For all test cases shown in this section, we fix $\Delta t = 0.1$ and the spatial meshsize $h = 1/50$; therefore, we have a total collection of $K = T/\Delta t$ such state vectors, where T is the terminal time.

To formulate the data assimilation problem for parameter estimation, we assume that we receive datasets

$$Y_{n+1} = H X_{n+1} + \xi_{n+1},$$

as the observational process with linear dependence on X_{n+1} and ξ_{n+1} is a noise following a Gaussian distribution. As we aim to learn the information about the fracture, we assume that the received data is directly related to the solution on the fracture. In particular, we have

$$H X_{n+1} = X_{\gamma, n+1},$$

where $X_{\gamma,n+1} = \left(\boldsymbol{u}_{h,\gamma}^{n+1}, p_{h,\gamma}^{n+1}\right)$ is the solution on the fracture at time instant $n+1$. As the width of the fracture in general is significantly small compared to the overall size of the domain of calculation, instead of approximating d, we denote $\theta := 1/d$ to be the parameter of interest,

and we add noise to θ to make it a stochastic process. The introduction of additional noise to the parameter of interest will transform it into an ensemble. As such, data assimilation techniques such as particle methods can be applied to facilitate the state estimation of those parameters. All together, we obtain the following optimal filtering problem for the parameter estimation task:

$$\theta_{n+1} = \theta_n + \epsilon_n, \tag{33}$$

$$Y_{n+1} = H\mathbf{\Phi}\big(H^{-1}(Y_n),\ 1/\theta_{n+1}\big) + \xi_{n+1}. \tag{34}$$

Note that Eqs. (33) and (34) are derived from the system (8) and (9) for the case with a single fracture. Similar reduced fracture models can be extended readily to the other test cases presented in this section, and the corresponding parameter estimation system can then be formulated. In what follows, we consider three different test cases with different settings of the fractures to study the applicability of the direct filter method to estimate the parameter of interest.

4.2 Test Case 1: One Single Fracture

For the first test case, the domain of calculation $\Omega = (0, 2) \times (0, 1)$ is divided into two equally sized subdomains by a fracture of width $d = 0.001$ parallel to the y-axis (see Fig. 2). For the boundary conditions, we impose $p = 1$ at the bottom and $p = 0$ at the top of the fracture. On the external boundaries of the subdomains, a no-flow boundary condition is imposed except on the lower fifth (length 0.2) of both lateral sides where a Dirichlet condition is imposed: $p = 1$ on the right, and $p = 0$ on the left. In Fig. 3, the snapshots of the pressure and velocity fields at final time $T = 5$ are shown to illustrate the behavior of the solutions.

In this test case, we choose $M = 80$ particles to empirically approximate the distribution of the unknown parameter and let ξ_n in Eq. (34) be $\xi_n \sim \mathcal{N}(0, 500)$. We also consider two sets of noise $\bar{\epsilon} = \{\bar{\epsilon}_n\}$ and $\tilde{\epsilon} = \{\tilde{\epsilon}_n\}$ in Eq. (33), where $\bar{\epsilon}_n \sim \mathcal{N}(0, 400)$ and $\tilde{\epsilon}_n \sim \mathcal{N}(0, 800)$. Finally, we denote $\bar{\rho} = \{1/\bar{\theta}_n\}$ and $\tilde{\rho} = \{1/\tilde{\theta}_n\}$ to be the sets of parameters obtained from the direct filter method corresponding to the noise $\bar{\epsilon}$ and $\tilde{\epsilon}$, respectively.

We present in Fig. 4 the estimation for d for each set of noise. We observe that both cases give accurate approximations for the true value d. Moreover, the direct filter $\tilde{\rho}$ tends to the true value of d after 30 steps, which is faster than the direct filter parameters $\bar{\rho}$ (around 40 steps). This means that increasing the range of the noise, which is equivalent to increasing the exploration rate for the parameters, may accelerate the convergence speed of the algorithm.

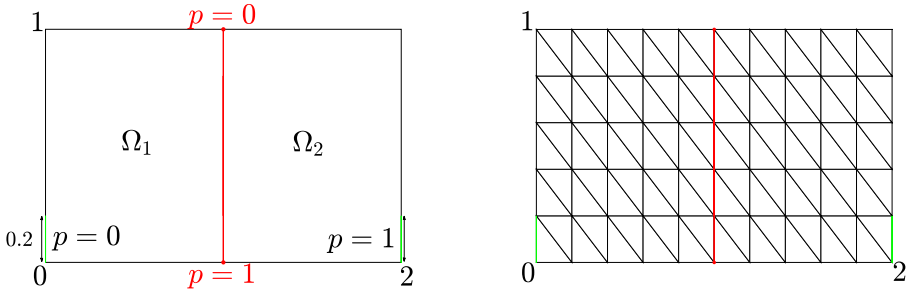

FIG. 2: [Test case 1] (Left) Geometry and boundary conditions of the test case. (Right) Example of a uniform triangular mesh for spatial discretization.

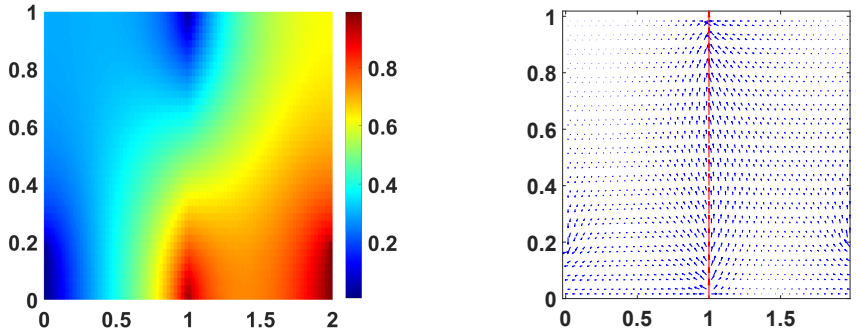

FIG. 3: [Test case 1] Pressure field (left) and velocity field (right) at time $T = 5$

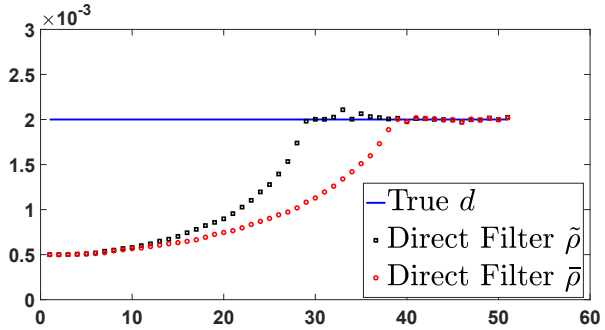

FIG. 4: [Test case 1] The estimations for d

4.3 Test Case 2: Two Parallel Fractures

In the second test case, we consider the domain of calculation being divided into three subdomains by two thin fractures γ_1 and γ_2, whose widths are $d_1 = 2.5e-03$ and $d_2 = 5e-03$, respectively. The boundary conditions are the same as in Test case 1, with additional boundary conditions imposed on the second fracture γ_2 (see Fig. 5). We note the the reduced fracture model (3) and (4), and its discretization (8) and (9) can be extended straightforwardly to this case.

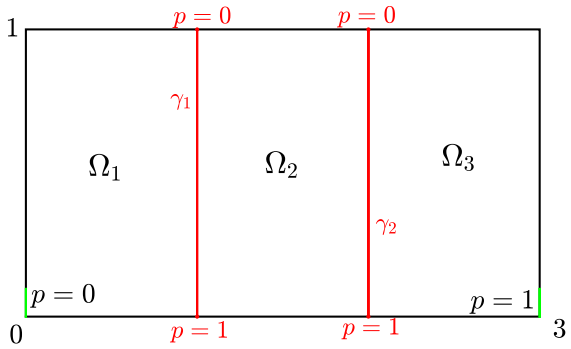

FIG. 5: [Test case 2] Geometry and boundary conditions of the test case

We aim to approximate d_1 and d_2 using the direct filter algorithm. The parameter θ in Eq. (33) is now a vector given by $\theta = (1/d_1, 1/d_2)$. We still choose the number of particles M to be 80 and $\xi_n \sim \mathcal{N}(0, 500)$. On the other hands, to accurately approximate both parameters, we need to choose bigger exploration rates. In particular, we consider two sets of noise $\bar{\epsilon} = \{\bar{\epsilon}_n\}_n = \{(\bar{\epsilon}_{1,n}, \bar{\epsilon}_{2,n})\}_n$ and $\tilde{\epsilon} = \{\tilde{\epsilon}_n\}_n = \{(\tilde{\epsilon}_{1,n}, \tilde{\epsilon}_{2,n})\}_n$, where $\bar{\epsilon}_{k,n}$ and $\tilde{\epsilon}_{k,n}$ are the noises corresponding to the filtering particles for $d_k,\ k = 1, 2$ with $\bar{\epsilon}_n \sim \mathcal{N}(0, \text{diag}(2000, 7000))$ and $\tilde{\epsilon}_n \sim \mathcal{N}(0, \text{diag}(4000, 8000))$. Finally, we denote by $\bar{\rho} = (\bar{\rho}_1, \bar{\rho}_2)$ and $\tilde{\rho} = (\tilde{\rho}_1, \tilde{\rho}_2)$ the particle estimates corresponding to the noise $\bar{\epsilon}$ and $\tilde{\epsilon}$, respectively.

We can observe from Fig. 6 that in both cases, the particles provide nearly identical approximations for the true values of d_1 and d_2. Similar to Test case 1, bigger exploration rates lead to faster convergence speed. For example, it took 30 steps for $\tilde{\epsilon}$ to approach the true value of d_1, while nearly 47 steps were required for $\bar{\epsilon}$ to reach the same value. We also remark that increasing the exploration rates does not significantly raise the computational cost, so the method's efficiency remains preserved.

4.4 Test Case 3: Two Intersecting Fractures

We consider a test case adapted from Alboin et al. (2002) where the domain of calculation is divided into four subdomains $\Omega_k, k = 1, \ldots, 4$ by two intersecting fractures Γ_1 and Γ_2, whose widths are $d_1 = 1e-03$ and $d_2 = 6e-04$, respectively. To write the reduced model in this case, we further partition each fracture into two smaller parts: $\Gamma_1 = \gamma_1 \cup \gamma_3$ and $\Gamma_2 = \gamma_2 \cup \gamma_4$ (see Fig. 7). The boundary conditions are given in Fig. 7. The reduced fracture model is then a coupled system between the four diffusion equations on $\Omega_k, k = 1, \ldots, 4$ and the four tangential PDEs on $\gamma_k, k = 1, \ldots, 4$.

For each $k = 1, \ldots, 4$, denote by $Z^n_{h,k} = \left(\boldsymbol{u}^n_{h,k},\ p^n_{h,k}\right)$ the solution on Ω_k and by $Z^n_{h,\gamma_k} = \left(\boldsymbol{u}^n_{h,\gamma_k},\ p^n_{h,\gamma_k}\right)$ the solution on γ_k at time instant n. The solution X_n at time instant n is given by $X_n = \left(Z^n_{h,k},\ Z^n_{h,\gamma_k}\right)_{k=1,\ldots,4}$, and the noisy observational data can be written as

$$Y_{n+1} = \left(Z^n_{h,\gamma_k}\right)_{k=1,\ldots,4} + \boldsymbol{\xi}_{n+1} = \left(Z^n_{h,\gamma_k}\right)_{k=1,\ldots,4} + \left(\xi^k_{n+1}\right)_{k=1,\ldots,4}.$$

The vector of targer parameters θ is set to be the same as Test case 2, which is $\theta = (1/d_1, 1/d_2)$, and the noise ϵ_n in Eq. (33) also consists of two components $\epsilon_n = (\epsilon_{1,n}, \epsilon_{2,n})$. Unlike Test case 2, we need to impose additional conditions at the intersection point of Γ_1 and Γ_2. Since the permeability in the fractures is considered to be much larger than the one in the

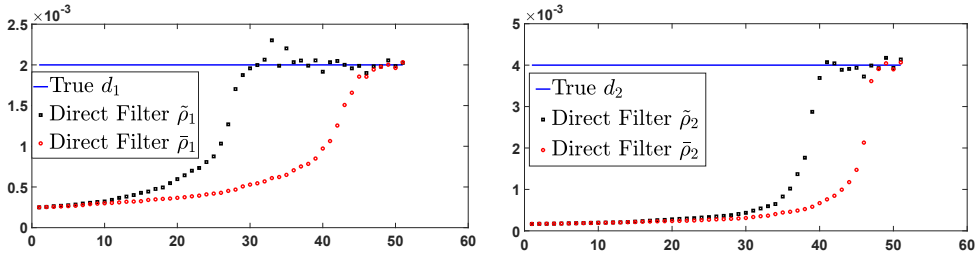

FIG. 6: [Test case 2] The estimations for d_1 [left] and d_2 [right]

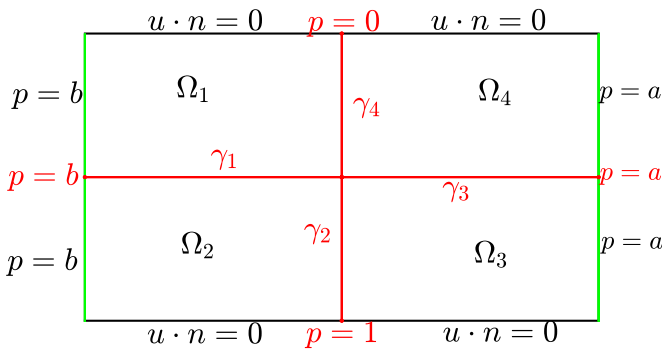

FIG. 7: [Test case 3] Geometry and boundary conditions of the test case

subdomains, we can impose the following boundary conditions at the intersection point (Alboin et al., 2002; Amir et al., 2021; Formaggia et al., 2014):

$$p^n_{h,\gamma_1} = p^n_{h,\gamma_2} = p^n_{h,\gamma_3} = p^n_{h,\gamma_4}, \qquad u^n_{h,\gamma_1} + u^n_{h,\gamma_2} + u^n_{h,\gamma_3} + u^n_{h,\gamma_4} = 0.$$

These conditions express the continuity of the pressure and the normal fluxes on the fractures across the intersection point.

We consider two sets of boundary conditions for Test case 3. For the first set, we let $a = 1$ and $b = 0$, which leads to Test case 3a. We show the snapshot of the solution for Test case 3a in Fig. 8. We can observe that the magnitude of the fluxes on the two fractures are relatively the same, and they flow in the direction driven by the boundary conditions. For Test case 3a, we fix the number of particles to be $M = 120$ and choose $\epsilon_n \sim \mathcal{N}(0, \text{diag}(8000, 10{,}000))$ and present the direct filter estimations for $\rho_1 = 1/\theta_1$ and $\rho_2 = 1/\theta_2$ in Fig. 9. With the chosen noise, we can see that the parameters converge to the true values relatively fast. We observed that the rate of convergence of ρ_2 is slower than that of ρ_1. It can be explained that the flow in the vertical fracture is a combination between the vertical flow in the fracture and the flow from the right subdomain. This mixed information may cause the parameter d_2 to be less sensitive so that the convergence rate is slower.

Next, we consider a different set of boundary conditions where $a = 5$ and $b = 0$, which leads us to Test case 3b. The snapshot of the solution for this test case is shown in Fig. 10. We can see that the flux in the horizontal fracture dominates the vertical one, which drives the flux on the

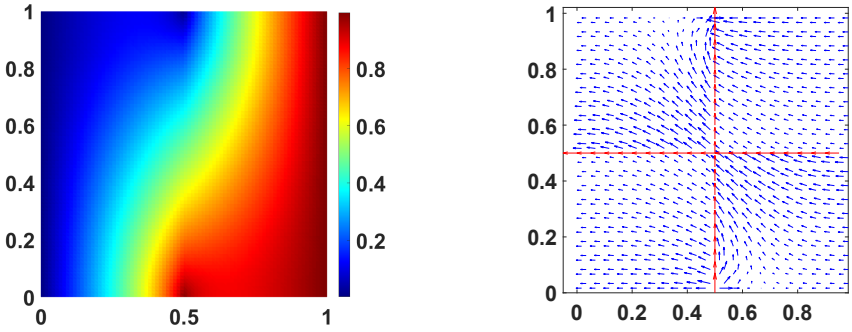

FIG. 8: [Test case 3a] Pressure field (left) and velocity field (right) for $a = 1$ and $b = 0$ at time $T = 5$

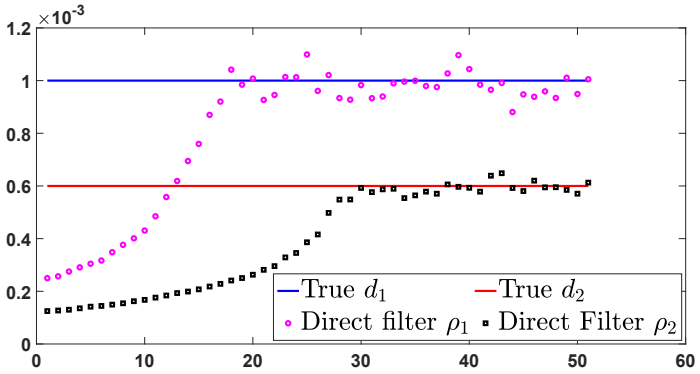

FIG. 9: [Test case 3a] The estimations for d_1 and d_2

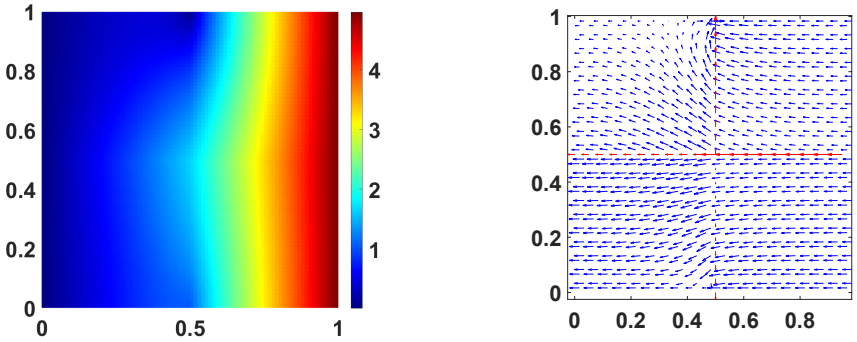

FIG. 10: [Test case 3b] Pressure field (left) and velocity field (right) for $a = 5$ and $b = 0$

lower part of the vertical fracture to flow in the opposite direction compared to Test case 3a. For this test case, to accurately approximate the values of d_1 and d_2, we need to choose large values for the noise, which is $\epsilon_n \sim \mathcal{N}(0, \text{diag}(18{,}000, 18{,}000))$. The parameter estimates are presented in Fig. 11. Again, we observe that the convergence rate of ρ_2 is slower than that of ρ_1 due to d_2 being less sensitive than d_1. However, similar to the previous test cases, the convergence speeds of the parameters to the exact values are relatively fast.

5. CONCLUSION

In this work, we studied the inverse problem of estimating the widths of the fractures in a fractured porous medium based on observations of the fluid flow in the rock matrix. A reduced fracture model was introduced and was fully discretized to serve as the forward problem of the model inversion. The inverse problem was then solved by using an online parameter estimation technique by adopting the direct filter method developed in Archibald et al. (2019). We presented several numerical experiments to show that the parameters of interest can be recovered accurately by our method under various circumstances. For the future work, we aim to extend our work to a more general goal where a complete characterization of a fracture can be inferred based on the observational data in the porous medium.

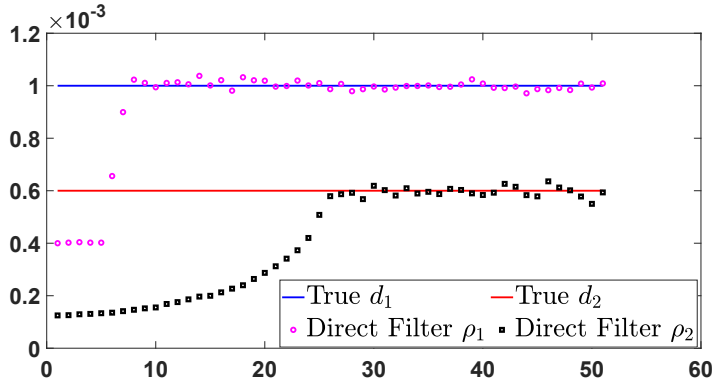

FIG. 11: [Test case 3b] The estimations for d_1 and d_2

REFERENCES

Alboin, C., Jaffré, J., and Roberts, J.E., and Serres, C., Domain Decomposition for Flow in Fractured Porous Media, *Domain Decomposition Methods in Science and Engineering*, C.H. Lai, P.E. Bjorstad, M. Cross, and O.B. Widlund, Eds., Bergen, Norway: Domain Decomposition Press, pp. 365–373, 1999.

Alboin, C., Jaffre, J., Roberts, J.E., and Serres, C., Modeling Fractures as Interfaces for Flow and Transport in Porous Media, *Fluid Flow and Transport in Porous Media: Mathematical and Numerical Treatment*, Vol. 295, South Hadley, MA: Contemporary Mathematics, pp. 13–24, 2002.

Ameur, H.B., Chavent, G., Cheikh, F., Clément, F., Martin, V., and Roberts, J.E., First-Order Indicators for the Estimation of Discrete Fractures in Porous Media, *Inverse Prob. Sci. Eng.*, vol. **26**, no. 1, pp. 1–32, 2018.

Ameur, H.B., Chavent, G., and Jaffré, J., Refinement and Coarsening Indicators for Adaptive Parametrization: Application to the Estimation of Hydraulic Transmissivities, *Inverse Prob.*, vol. **18**, no. 3, pp. 775–794, 2002.

Amir, L., Kern, M., Mghazli, Z., and Roberts, J.E., Intersecting Fractures in Porous Media: Mathematical and Numerical Analysis, *Appl. Anal.*, vol. **102**, pp. 1312–1334, 2021.

Angot, P., Boyer, F., and Hubert, F., Asymptotic and Numerical Modelling of Flows in Fractured Porous Media, *M2AN Math. Model. Numer. Anal.*, vol. **43**, no. 2, pp. 239–275, 2009.

Archibald, R. and Bao, F., Kernel Learning Backward SDE Filter for Data Assimilation, *J. Comput. Phys.*, vol. **455**, no. 3, p. 111009, 2022.

Archibald, R., Bao, F., and Tu, X., A Direct Method for Parameter Estimations, *J. Comput. Phys.*, vol. **398**, p. 108871, 2019.

Bao, F., Cao, Y., and Han, X., An Implicit Algorithm of Solving Nonlinear Filtering Problems, *Commun. Math. Sci.*, vol. **16**, no. 2, pp. 382–402, 2014.

Bao, F., Cao, Y., and Zhao, W., A Backward Doubly Stochastic Differential Equation Approach for Nonlinear Filtering Problems, *Commun. Comput. Phys.*, vol. **23**, no. 5, pp. 1573–1601, 2018.

Bao, F., Cao, Y., and Chi, H., Adjoint Forward Backward Stochastic Differential Equations Driven by Jump Processes and Its Application to Nonlinear Filtering Problems, *Int. J. Uncertain. Quan.*, vol. **9**, no. 2, pp. 143–159, 2019.

Bao, F., Cao, Y., and Han, X., Forward Backward Doubly Stochastic Differential Equations and Optimal Filtering of Diffusion Processes, *Commun. Math. Sci.*, vol. **18**, no. 3, pp. 635–661, 2020.

Bao, F. and Maroulas, V., Adaptive Meshfree Backward SDE Filter, *SIAM J. Sci. Comput.*, vol. **39**, no. 6, pp. A2664–A2683, 2017.

Boffi, D., Brezzi, F., and Fortin, M., *Mixed Finite Elements Methods and Applications*, Heidelberg: Springer, 2013.

Brezzi, F. and Fortin, M., *Mixed and Hybrid Finite Element Methods*, Berlin: Springer, 1991.

Cogan, N., Bao, F., Paus, R., and Dobreva, A., Data Assimilation of Synthetic Data as a Novel Strategy for Predicting Disease Progression in Alopecia Areata, *Math. Med. Biol.: J. IMA*, vol. **38**, no. 3, pp. 314–332, 2021.

Dai, Z. and Samper, J., Inverse Problem of Multicomponent Reactive Chemical Transport in Porous Media: Formulation and Applications, *Water Resour. Res.*, vol. **40**, p. W07407, 2004.

Doucet, A., de Freitas, N., and Gordon, N., An Introduction to Sequential Monte Carlo Methods, *Sequential Monte Carlo Methods in Practice*, New York: Springer, pp. 3–13, 2001a.

Doucet, A., de Freitas, N., and Gordon, N., *Sequential Monte Carlo Methods in Practice*, New York: Springer, 2001b.

Dyck, O., Ziatdinov, M., Jesse, S., Bao, F., Nobakht, A.Y., Maksov, A., Sumpter, B.G., Archibald, R., Law, K.J.H., and Kalinin, S.V., Probing Potential Energy Landscapes via Electron-Beam-Induced Single Atom Dynamics, *Acta Materialia*, vol. **203**, p. 116508, 2021.

Formaggia, L., Fumagalli, A., Scotti, A., and Ruffo, P., A Reduced Model for Darcy's Problem in Networks of Fractures, *ESAIM: Math. Model. Numer. Anal.*, vol. **48**, pp. 1089–1116, 2014.

Fumagalli, A. and Scotti, A., Numerical Modeling of Multiphase Subsurface Flow in the Presence of Fractures, *Commun. Appl. Ind. Math.*, vol. **3**, pp. 1–23, 2011.

Gander, M.J., Hennicker, J., and Masson, R., Modeling and Analysis of the Coupling in Discrete Fracture Matrix Models, *SIAM J. Numer. Anal.*, vol. **59**, no. 1, pp. 195–218, 2021.

Goc, R.L., de Dreuzy, J.R., and Davy, P., An Inverse Problem Methodology to Identify Flow Channels in Fractured Media Using Synthetic Steady-State Head and Geometrical Data, *Adv. Water Resour.*, vol. **33**, no. 7, pp. 782–800, 2010.

Gwo, J.P., In Search of Preferential Flow Paths in Structured Porous Media Using a Simple Genetic Algorithm, *Water Resour. Res.*, vol. **37**, no. 6, pp. 1589–1601, 2001.

Hoang, T.T.P., Japhet, C., Jaffré, J., Kern, M., and Roberts, J.E., Space-Time Domain Decomposition Methods for Diffusion Problems in Mixed Formulations, *SIAM J. Numer. Anal.*, vol. **51**, no. 6, pp. 3532–3559, 2013.

Hoang, T.T.P., Japhet, C., Kern, M., and Roberts, J.E., Space-Time Domain Decomposition for Reduced Fracture Models in Mixed Formulation, *SIAM J. Numer. Anal.*, vol. **54**, no. 1, pp. 288–316, 2016.

Hoang, T.T.P., Japhet, C., Kern, M., and Roberts, J.E., Space-Time Domain Decomposition Methods for Advection-Diffusion Problems in Mixed Formulations, *Math. Comput. Simul.*, vol. **137**, pp. 366–389, 2017.

Huynh, P.T., Hoang, T.T.P., and Cao, Y., Fast and Accuracy-Preserving Domain Decomposition Methods for Reduced Fracture Models with Nonconforming Time Grids, *J. Sci. Comput.*, vol. **96**, no. 23, 2023a. DOI: 10.1007/s10915-023-02251-0

Huynh, P.T., Hoang, T.T.P., and Cao, Y., Operator Splitting and Local Time-Stepping Methods for Transport Problems in Fractured Porous Media, *Commun. Comput. Phys.*, vol. **34**, no. 5, pp. 1215–1246, 2023b.

Huynh, P.T., Hoang, T.T.P., and Cao, Y., Monolithic and Local Time-Stepping Decoupled Algorithms for Transport Problems in Fractured Porous Media, *IMA J. Numer. Anal.*, 2024. DOI: 10.1093/imanum/drae005

Jaffre, J., Martin, V., and Roberts, J.E., Modeling Fractures and Barriers as Interfaces for Flow in Porous Media, *SIAM J. Sci. Comput.*, vol. **26**, pp. 1667–1691, 2005.

Kadeethum, T., Nick, H., Lee, S., and Ballarin, F., Flow in Porous Media with Low Dimensional Fractures by Employing Enriched Galerkin Method, *Adv. Water Resour.*, vol. **142**, p. 103620, 2020.

Kantas, N., Doucet, A., Singh, S., Maciejowski, J., and Chopin, N., On Particle Methods for Parameter Estimation in State-Sapce Models, *Stat. Sci.*, vol. **30**, no. 3, pp. 328–351, 2015.

Krause, M., Krevor, S., and Benson, S., A Procedure for the Accurate Determination of Sub-Core Scale Permeability Distributions with Error Quantification, *Transp. Porous Media*, vol. **98**, pp. 565–588, 2013.

Liu, J. and West, M., Combined Parameter and State Estimation in Simulation-Based Filtering, *Sequential Monte Carlo in Practice*, A. Doucet, N. de Freitas, and N. Gordon, Eds., New York: Springer, pp. 197–223, 2001.

Mauldon, A.D., Karasaki, K., Martel, S.J., Long, J.C.S., Landsfeld, M., and Mensch, A., An Inverse Technique for Developing Models for Fluid Flow in Fracture Systems Using Simulated Annealing, *Water Resour. Res.*, vol. **29**, no. 11, pp. 3775–3789, 1993.

Morales, F. and Showalter, R.E., Interface Approximation of Darcy Flow in a Narrow Channel, *Math. Methods Appl. Sci.*, vol. **35**, pp. 182–195, 2012.

Morzfeld, M., Day, M.S., Grout, R.W., Pau, G.S.H., Finsterle, S.A., and Bell, J.B., Iterative Importance Sampling Algorithms for Parameter Estimations, *SIAM J. Sci. Comput.*, vol. **40**, no. 2, pp. B329–B352, 2018.

Neuman, S.P. and Yakowitz, S., A Statistical Approach to the Inverse Problem of Aquifer Hydrology: 1. Theory, *Water Resour. Res.*, vol. **15**, no. 4, pp. 845–860, 1979.

Renshaw, C.E., Estimation of Fracture Zone Geometry from Steady-State Hydraulic Head Data Using Iterative Sequential Cokriging, *Geophys. Res. Lett.*, vol. **23**, no. 19, pp. 2685–2688, 1996.

Roberts, J. and Thomas, J.M., Mixed and Hybrid Methods, *Finite Element Methods (Part 1)*, Amsterdam: Elsevier, pp. 523–639, 1991.

Sun, H., Moore, N.J., and Bao, F., Parameter Estimation for the Truncated KdV Model through a Direct Filter Method, *J. Mach. Learn. Model. Comput.*, vol. **4**, no. 1, pp. 109–132, 2023.

Wei, Y.J. and Rabinovich, A., The Inverse Problem of Permeability Identification for Multiphase Flow in Porous Media, *Phys. Fluids*, vol. **35**, no. 7, p. 073327, 2023.

West, M., Approximating Posterior Distribution by Mixture, *J. R. Stat. Soc.*, vol. **54**, pp. 553–568, 1993.